This manuscript has been accepted for publication in Earth and Planetary Science Letters. The manuscript will undergo copyediting, typesetting, and review of the resulting proof before it is published in its final form. Please note that during the production process errors may be discovered which could affect the content, and all disclaimers that apply to the journal apply to this manuscript. A definitive version was subsequently published in Earth and Planetary Science Letters, V. 245, pp. 1-11, DOI: 10.1016/j.epsl.2015.05.043

Quantification of the CO_2 budget and H_2O-CO_2 systematics in subduction-zone magmas through the experimental hydration of melt inclusions in olivine at high H_2O pressure

Nikita Mironov[1], Maxim Portnyagin[1,2*], Roman Botcharnikov[3], Andrey Gurenko[4], Kaj Hoernle[2], and Francois Holtz[3]

1- V.I. Vernadsky Institute of geochemistry and analytical chemistry, Kosygin 19, 119991 Moscow, Russia

2- GEOMAR Helmholtz Center for Ocean Research Kiel, Wischhofstrasse 1-3, 24148 Kiel, Germany

3- Institut für Mineralogie, Leibniz Universität Hannover, Callinstr. 3, 30167, Hannover, Germany

4- Centre de Recherches Pétrographiques et Géochimiques, UMR 7358, Université de Lorraine, 54501 Vandoeuvre-lès-Nancy, France

*Corresponding author (mportnyagin@geomar.de)

Key words:
melt inclusion, olivine, experiment, volatiles, Kamchatka

Received at Editorial Office: 30 Dec 2014

Article revised: 21 May 2015

Article accepted for publication: 22 May 2015

HIGHLIGHTS:

- Melt inclusions from Klyuchevskoy were homogenized at 1150 ^{o}C and P_{H2O} = 500 MPa.
- High-P experiments can recover initial H_2O and CO_2 contents in dehydrated inclusions.
- Isothermal (de)hydration results in linear trend of CO_2 and H_2O in inclusion glasses.
- Parental Klyuchevskoy magmas contain ~3800 ppm CO_2 and 4-5 wt.% H_2O.
- At least 80% of CO_2 is slab-derived in the Klyuchevskoy magmas with CO_2/Nb ~3000.

ABSTRACT

Reliable evaluation of CO_2 contents in parental arc magmas, which can be preserved in melt inclusions in phenocrysts, is required to verify the proposed efficiency of CO_2 recycling at convergent margins. Quantification of bulk CO_2 concentration in melt inclusions requires their complete homogenization. Using samples from lavas from the Bulochka vent of Klyuchevskoy Volcano (Kamchatka), we applied a novel experimental approach to homogenize and re-equilibrate naturally dehydrated (<1 wt.% H_2O) melt inclusions from high-Fo (85-91 mol.%) olivine. The experiments were performed at temperatures of 1150-1400 ^oC, pressures of up to 500 MPa, under dry to H_2O-saturated conditions and with oxygen fugacity ranging from CCO to QFM+3.3. No homogenization was achieved at dry conditions. Complete dissolution of fluid bubbles (homogenization) in the melt inclusions was achieved at H_2O pressures of 500 MPa and temperature of 1150 ^oC, when water content in the melt inclusions reached 4-5 wt.% H_2O. The CO_2 content in the homogenized inclusions is 3800±140 ppm and CO_2/Nb = 3000±420, which are the highest values reported so far for the typical middle-K primitive arc melts and fall within the range of values inferred from the magmatic flux and volcanic gas data for primary arc magma compositions. About 80-85% of the CO_2 in Klyuchevskoy magmas is likely to be derived from the subducting slab and can be attributed to flux melting with a fluid having a CO_2/H_2O ratio of ~0.06. The H_2O and CO_2 contents in the melt inclusions after hydrous experiments were found to correlate positively with each other and negatively with the volume of fluid bubble, reflecting increasing internal pressure in melt inclusions with increasing melt hydration. Therefore, similar trends observed in some natural sets of melt inclusions can be attributed to a partial dehydration of melts after entrapment, operating simultaneously with or following post-entrapment crystallization. Our study implies that the process of post-entrapment dehydration can be completely reversed under high pressure experimental conditions. If temperature, redox conditions and pressure of melt inclusion entrapment can be independently estimated, then our novel experimental approach (homogenization at high H_2O pressure) can be used to reconstruct the initial CO_2 content and also the entire composition of melt inclusions in olivine, including their initial H_2O content, from any type of volcanic rock. With this approach volatiles in ancient lavas can also be determined, expanding our knowledge of volatile recycling further back in Earth history.

1. Introduction

Magmatic and hydrothermal processes at convergent plate margins represent an important component of the global carbon cycle. At such margins large amounts of CO_2 in sediments and oceanic crust are subducted into the mantle and partially returned to the exosphere by arc volcanism (e.g., Marty and Tolstikhin, 1998; Hilton et al., 2002). The median $CO_2/^3He$ ratio in volcanic arc gases is higher than that in normal mid-ocean-ridge basalt (N-MORB) by a factor of ~8, suggesting that arc magmas are enriched in CO_2 compared to MORB and contain at least 80% recycled slab-derived CO_2 (Marty and Tolstikhin, 1998). C-isotope systematics of volcanic gases indicate an even higher amount of slab-derived CO_2 (88-97% for 7 arcs, including Kamchatka; Hilton et al., 2002). The absolute amounts of CO_2 in parental arc magmas, however, are poorly constrained. The available indirect estimates from CO_2 volcanic gas fluxes and magma emplacement rates in arcs range from 0.3-1.3 wt.% CO_2 (Wallace, 2005; Fischer and Marty, 2005; Shinohara, 2013). Independent and reliable evaluation of CO_2 contents in parental arc magmas is required to verify the proposed volatile fluxes, efficiency of CO_2 recycling and crustal growth rates at convergent margins.

Experimental studies demonstrate that solubility of CO_2 in silicate melts decreases strongly with decreasing pressure (e.g., Blank and Brooker, 1994). In addition, CO_2 partitions into the fluid phase as soon as magmas start to degas. Therefore, CO_2 is commonly lost through exsolution into coexisting magmatic fluids during magma ascent and eruption. The only direct approach for quantifying the primary CO_2 content in magmas is to study melt inclusions (MIs) in minerals, which represent small droplets of melt trapped by growing crystals at depth (e.g., Roedder, 1984; Wallace, 2005). The available database of CO_2 content in MIs from subduction-related settings consists of ~1700 analyses (GEOROC, 2014). The CO_2 concentrations range from below the detection limit to 5300 ppm, with about 90% of

87 inclusions having <500 ppm CO_2 (Fig. 1). The highest concentrations of CO_2 in MIs were
88 reported for basalts of Etna Volcano, Italy (≥3280 ppm, Kamenetsky et al., 2007) and for
89 basanites from Colima volcanic complex in Mexico (5300 ppm, Vigouroux et al., 2008).
90 However, the Etna and Colima rocks have major and trace element compositions, which are
91 quite different from middle-K calc-alkaline arc rocks (e.g., Kelemen et al., 2003). None of the
92 published CO_2 contents in MIs from typical arc rocks is consistent with the large CO_2 output
93 from volcanic arcs inferred from volcanic gas data (Wallace, 2005; Shinohara et al., 2013)
94 (Fig. 1).

95 The majority of studied MIs formed during the late stages of magma evolution at shallow
96 depths and therefore the minerals trapped already strongly degassed melts with low CO_2
97 contents (e.g., Wallace, 2005). Primitive MIs trapped in high-Fo olivine (Fo>85 mol.%) are
98 rare in the existing database. Such inclusions are usually significantly modified after
99 entrapment during cooling and decompression and always contain a fluid (gas) bubble (e.g.,
100 Anderson and Brown, 1993; Danyushevsky et al., 2002). Thermodynamic modeling (Steele-
101 MacInnes et al., 2011) and several studies of natural inclusions (e.g., Anderson and Brown,
102 1993; Kamenetsky et al., 2002; 2007; Hartley et al., 2014; Wallace et al., 2015; Moore et al.,
103 2015) have demonstrated that the bubbles can comprise a major fraction (80% or more) of
104 the initial CO_2 content in the MIs, explaining the low CO_2 concentrations measured in the
105 coexisting glasses.

106 Estimation of the bulk CO_2 content in bubble-bearing MIs is possible through two
107 different approaches. According to one approach, the bulk CO_2 content is calculated by mass
108 balance using volume proportions of fluid and glass in MIs and the amount of CO_2 stored in
109 them. The amount of CO_2 in the fluid phase is calculated from the ideal gas equation and
110 saturation pressure at melt-glass transition (Shaw et al., 2010) or from the fluid density

measured by cryometry (Naumov et al., 2006) or by Raman spectroscopy (e.g., Hartley et al., 2014; Moore et al., 2015). This approach has a number of uncertainties arising from the determination of the fluid density (e.g., Hartley et al., 2014) and the volume proportions in MIs, which sometimes contain an excessive ("prisoner") fluid phase trapped with melt, and from the common precipitation of carbonates on the bubble wall (e.g., Kamenetsky et al., 2002; Moore et al., 2015). An alternative, direct approach is an experimental homogenization of MIs leading to a complete dissolution of CO_2 back into the melt and enabling the direct analysis of CO_2 concentration in the quenched glass (e.g., Wallace et al., 2015). Although this approach seems to be straightforward and easy, heating experiments with MIs from arc rocks performed at 1 atm often fail to dissolve the fluid bubble completely even during significant overheating (e.g., Danyushevsky et al., 2002).

In this study, we introduce a new experimental approach to homogenize MIs under high H_2O pressure. This approach was successfully applied to homogenize strongly dehydrated inclusions from Klyuchevskoy Volcano, Kamchatka and to estimate their initial CO_2 content. The results help to understand better MI evolution after entrapment and during experiments and suggest that the entire composition of MIs in olivine, including their initial H_2O and CO_2 contents, can be restored experimentally, if conditions of MI entrapment can be independently estimated.

2. Samples from Klyuchevskoy volcano

Melt inclusions were studied in olivine phenocrysts from a lava flow (sample K9-N27, 56.1526° N, 160.7939° E, 876 m) and tephra layer comprising 0.5-1 cm lapilli (sample K7-T1-51, 56.1464° N, 160.8241° E), both associated with the ~3 ky old Bulochka cone on the NE slope of Klyuchevskoy Volcano. These rocks are the most primitive from Klyuchevskoy (e.g.,

135 Khubunaya et al., 1994; Ariskin et al., 1995) (Table 1) and contain up to 10 vol.% olivine
136 phenocrysts with high-Mg (Fo_{87-91}) cores and outer 100-200 μm-wide rims of less magnesian
137 olivine (~Fo_{85}) (Fig. 2a).

138 The compositions of MI glasses from Bulochka samples have been reported in several
139 papers (Sobolev and Chaussidon, 1996; Churikova et al., 2007; Portnyagin et al., 2007b; Auer
140 et al., 2009; Mironov and Portnyagin, 2011). After reheating at 1 atm using the "Vernadsky"
141 stage (Danyushevsky et al., 2002), MIs in olivine from lava samples were shown to contain ≤1
142 wt.% H_2O and ≤274 ppm CO_2 (Churikova et al., 2007; Mironov and Portnyagin, 2011) and
143 were interpreted to be extensively dehydrated (>3 wt.% H_2O loss) due to slow cooling in the
144 lava flow (Portnyagin et al., 2008; Mironov and Portnyagin, 2011). Glasses of MIs from
145 Bulochka volcanic bombs and lapilli contain larger amounts of H_2O (1.1-4.0 wt.%) and CO_2
146 (up to 657 ppm) than those from lavas (Auer et al., 2009; Mironov and Portnyagin, 2011).

147 Glassy MIs from Bulochka lapilli studied here consisted of glass, fluid bubble (1-3
148 vol.%) and occasionally prisoner Cr-spinel (Fig. 2b; Table 1). The contents of H_2O (2.9-3.4
149 wt.%) and particularly CO_2 (880-1200 ppm) in these inclusions are quite high compared to
150 the previously published data, but lower than expected for the Klyuchevskoy parental melts
151 (~3.5-4.0 wt.% H_2O and ≥3500 ppm CO_2; Mironov and Portnyagin, 2011). The contents of
152 H_2O in the glassy MIs reveal a positive correlation with the MI sizes that implies a variable
153 H_2O loss from the inclusions after entrapment, providing the possibility to study the magma
154 ascent rate preceding the Bulochka eruption (Lloyd et al., 2013).

155 Temperature (T), oxygen fugacity (fO_2) and pressure (P) at MI entrapment in olivine
156 were estimated from the mineral equilibria and fluid inclusions. The temperature estimated
157 from the Al partitioning between olivine and spinel inclusions (Wan et al., 2008) ranges from
158 1150 to 1230 ^{o}C and reveals a reasonable positive correlation with olivine Fo-number (Fig.

159 3a, Table A.1). Oxygen fugacity was estimated to be ΔQFM = 0.8-1.8 from the spinel-olivine
160 equilibria (Ballhaus et al., 1990) (Fig. 3b). Crystallization pressure was assumed to be 500
161 MPa at 1150 ^{o}C as estimated from the cryometrically measured density of CO_2-rich fluid
162 inclusions (0.80-0.81 g/cm^3) in olivine Fo_{88} (Fig. 2c) from the Ochki lava flow, also from
163 Klyuchevskoy (Mironov and Portnyagin, 2011).
164
165 **3. Experimental and Analytical Methods**
166 The experiments were performed with partially crystallized and dehydrated MIs in
167 olivine grains of 0.5-1.25 mm size separated from Bulochka lava sample (Fig. 3d). The
168 experiments were conducted at the Institute of Mineralogy, Leibniz University in Hannover
169 (Germany) in vertically-oriented, internally-heated pressure vessels (IHPVs), which allow an
170 accurate control of T, P, fO_2 and rapid quenching of experimental products. In the present
171 study, we used 20x3 mm $Au_{80}Pd_{20}$ tubing welded on one side. The capsules were loaded
172 sequentially with a powdered matrix glass, 7-8 olivine grains containing MIs, distilled H_2O,
173 and powdered glass on top. The weight ratio of glass to olivine grains was 2.8-3.6. A
174 synthetic matrix glass was used with a composition similar to the Bulochka rocks (Table 1).
175 The amount of H_2O varied from 5 to 11.3 wt.% relative to the glass. One capsule was charged
176 with olivine grains and 20% NaCl aqueous solution only (#C4-4), and another capsule
177 contained olivine grains only, without any matrix glass or fluid (#C8-5) (Table 1). After
178 loading, the capsules were welded shut, weighed, heated at 110 ^{o}C for 1 hour, and weighed
179 again to check for leaks. Every experimental run series comprised 2-5 capsules placed next to
180 each other in the sample holder. The capsules were kept in IHPVs at temperatures of 1150-
181 1200 °C and pressures of 300-500 MPa for 24-28 hours and then quenched rapidly (~150
182 ^{o}C/sec). Nominal external oxygen fugacity varied during the experiments from the intrinsic

183 fO_2 of IHPV (QFM+3.3) at H_2O-saturated (Schuessler et al., 2008) to more reduced (QFM+0.6)
184 conditions when IHPV was pressurized by Ar-H_2 mixture. One additional experimental run
185 was performed with loose olivine grains in a graphite capsule (CCO redox buffer) at 1400 ^oC
186 and 1 atm for 1 hour (#C9).

187 After finishing the experiments, the olivine grains with MIs were extracted from the
188 capsules and prepared for further analytical studies. The MIs were first analyzed for CO_2 and
189 H_2O using secondary ion mass-spectrometry (SIMS, CAMECA IMS 1280 HR) in CRPG (Nancy,
190 France). The accuracy of SIMS analyses was estimated to be 17% for CO_2 and 9% for H_2O.
191 Then the inclusions were analyzed for major elements, S and Cl by electron microprobe
192 (JEOL JXA 8200) at GEOMAR (Kiel, Germany) and finally for selected trace elements (Ti, Nb,
193 Ba, La, Th) by SIMS (CAMECA IMS 4f) at the Yaroslavl Branch of the Institute of Physics and
194 Technology (Yaroslavl, Russia). The details of the analytical techniques can be found in
195 Appendix A.
196
197 **4. Results**
198 The olivine cores containing MIs revealed no compositional or textural changes after
199 the experiments. In the experiments with hydrous matrix melt, olivine rims exhibited some
200 minor dissolution features in addition to new, artificially formed secondary melt and fluid
201 inclusions. The outer rim of the olivines was replaced with ~10-20 μm inversely zoned olivine
202 with Fo-number ≤91.5 near the crystal-melt interface in runs at QFM+0.6 and ≤93 in runs at
203 QFM+3.3 (Table 1). Olivine rims in the runs with fluid only (no glass matrix) exhibited
204 recrystallization/dissolution features and contained a large number of secondary fluid
205 inclusions ± magnetite crystals. No compositional or textural changes were observed in
206 olivines in the experiments without fluid or glass matrix.

After experimental runs, the initially partly-crystallized inclusions (Fig. 2d) were composed of glass and fluid in variable proportions (Fig. 2e-h), except for MIs from the runs performed at 500 MPa. At this pressure, no fluid bubble was present in most MIs (Fig. 2i). In some inclusions, we observed small spinel crystals, which we interpret to be prisoner crystals trapped together with melt. Also, tiny sulfide globules were observed in some of the runs conducted at QFM+0.6 and CCO, resulting from sulfide saturation of the melt under relatively reducing conditions (Fig. 2 e,f).

All MIs heated under dry conditions (at 1 atm and 1400 ^{o}C and at 300 MPa and 1200 ^{o}C) contain fluid bubbles occupying 1.5 - 2.9 vol.% (Fig. 2e,f; Table 1). The CO_2 (<600 ppm) and H_2O (<1 wt.%) contents in the glasses are very close to those in MIs heated using a "Vernadsky stage" at 1 atm (Mironov and Portnyagin, 2011). MIs in olivines enclosed within a hydrous matrix (melt or fluid) were moderately to strongly hydrated (H_2O = 2.2-5.2 wt.%).

MIs in runs with a mixed H_2O-NaCl fluid and no melt matrix had intermediate H_2O (2.2-3.2 wt.%) and CO_2 (1510-2670 ppm) concentrations in the glasses and fluid bubbles occupying 0.8-1.3 vol.% (Fig. 2g, Fig. 4). These MIs have fluid bubble volumes and H_2O contents similar to natural glassy inclusions. The CO_2 and MgO contents of the MIs after experiments, however, are higher than in non-treated MIs (Table 1; Fig. 2b,g; Fig. 4).

The most significant hydration (3.3-5.2 wt.%) and enrichment of MI glasses in CO_2 (2580-3960 ppm), accompanied by a dramatic reduction of bubble volume down to 0-0.7 vol.%, was achieved in the experiments at 300 and 500 MPa, in which olivines interacted with hydrous matrix silicate melt (Fig. 4a-b). The concentrations of H_2O and CO_2 in the MI glass show strong positive near-linear correlations with each other, yet they correlate inversely with the fluid bubble volume. The highest CO_2 concentrations of 3780±140 ppm (1s, n=5) were obtained for the most hydrated and completely homogenized MIs in the run

231 performed at 500 MPa. In contrast to MIs, the concentrations of CO_2 in the experimental
232 matrix glasses are lower (70-520 ppm), whereas H_2O concentrations are higher (4.3-6.6
233 wt.%) (Fig. 4b).

234 Dissolution of olivine from MI walls in response to melt hydration at constant
235 temperature is illustrated by the correlation between MgO and H_2O in MI glasses (Fig. 4c).
236 Assuming an MgO of 4 wt.% in MIs before experiments, the amount of olivine that dissolved
237 into inclusions was estimated to be 11-17% in the runs at 1150 ^oC and high H_2O pressure
238 (Fig. 4c). The H_2O contents in most MIs are lower than in matrix glasses, apparently due to
239 incomplete re-equilibration of MIs with hydrous matrix with respect to H_2O during 24-hours-
240 long experiments. The MgO contents in MIs are also lower than in matrix glasses, reflecting
241 the dependence of MgO on H_2O content in melts equilibrated with olivine at constant
242 temperature (e.g., Putirka, 2008).

243 The calculated density of the melt, internal pressure inside MIs, and mole fraction of
244 CO_2 in the equilibrium fluid are shown in Fig. 4d,e,f, respectively, as a function of H_2O in the
245 experimentally treated MIs.

246

247 **5. Discussion**

248 **5.1 Initial CO_2 content in primary Klyuchevskoy magmas**

249 The concentration of CO_2 (3800±140 ppm) in the completely homogenized MIs
250 agrees very well with the minimal CO_2 concentration (3500 ppm) in the Klyuchevskoy
251 parental magmas deduced from the study of high density (0.81 g/cm^3), CO_2-rich fluid
252 inclusions in ~Fo_{88} olivines (Mironov and Portnyagin, 2011). These concentrations are about
253 two times higher than the maximum CO_2 values in previously published data for
254 Klyuchevskoy (<1900 ppm CO_2) (Auer et al., 2008; Mironov and Portnyagin, 2011), which

represent CO_2 concentrations in the residual glasses of bubble-bearing MIs and do not take into account the presence of CO_2 in an equilibrium fluid.

None of the experimentally treated Bulochka MIs with high CO_2 concentration contain a large (>1 vol.%) fluid bubble after the experiments (Table 1). If a large gas volume had still been present after the experimental treatment, a significant fraction of CO_2 (>2000 ppm) would remain undissolved in the melt, which is not the case (Fig. 4a,b). Therefore, our new data do not provide evidence that magmas with CO_2 content significantly exceeding 3500-4000 ppm existed in the Klyuchevskoy plumbing system, assuming that the analyzed olivines represent the earliest phases which crystallized and that degassing did not occur before the onset of olivine crystallization. The Bulochka samples have typical trace element compositions for recent Klyuchevskoy magmas (accessible and studied lavas date back to <3.5 ka, V. Ponomareva, personal communication). For example, Ba/La ratio, often used as a proxy for H_2O fluid flux from the subducted slab (e.g. Sadofsky et al., 2008), is similar in Bulochka MIs and host rocks (Ba/La=43-57 and 50-53, respectively; Table 1) and is well within the range of Klyuchevskoy magmas (Ba/La=52±16, 2s, n=52; Portnyagin et al., 2007a). The measured CO_2 concentrations in the homogenized Bulochka MIs can thus provide valuable insights into the compositions of primary Klyuchevskoy magmas and their source(s).

The CO_2 concentrations in the homogenized MIs are among the highest ever reported for melt inclusions from subduction-related settings globally (Fig. 1) and fall within the range of the expected CO_2 contents in typical primary arc magmas (>3000 ppm, e.g. Wallace, 2005), estimated using the annual CO_2 flux from arc volcanoes and an estimate of the global rate of addition of mafic magma to arcs. Although the CO_2 contents are lower than the range of CO_2 in the parental arc magmas of 6000-13000 ppm preferred by Wallace (2005), they are very close to the most recent and lower estimate of the average CO_2 content in primary arc

magmas (~3700 ppm), based on the updated ^{3}He flux (65 mol/y) and crustal growth rate of 2.7 km^3/y in subduction zones (Shinohara, 2013).

Furthermore, the homogenized Klyuchevskoy MIs have exceptionally high CO_2/Nb = 3000±420 (Fig. 5a), which exceeds by about 5-6 times the CO_2/Nb ratio in the Depleted MORB Mantle (DMM, CO_2/Nb = 505±168; Rosenthal et al., 2015), an appropriate source for the Klyuchevskoy parental magmas (Portnyagin et al., 2007b). At degrees of mantle melting exceeding a few percent in a closed system, CO_2 and Nb do not fractionate from each other (Rosenthal et al., 2015) (Fig. 5). Assuming negligible amount of Nb in the slab component and 0.149 ppm Nb in DMM (Workman and Hart, 2005), the 5-6 time enrichment of the CO_2/Nb ratio in the studied MIs indicates a contribution of slab component to the CO_2 budget in Klyuchevskoy magmas of ~83%. The contribution could be even larger, if the slab-derived component contained some Nb, as would be expected in a hydrous slab melt or a supercritical fluid (Portnyagin et al., 2007a,b). The inferred slab contribution thus approaches closely the estimates from $CO_2/^{3}He$ and C-isotope systematics of volcanic arc gases, which indicate that 80-97% of the carbon in the arc magmas is derived from the slab (Marty and Tolstikhin, 1998; Hilton et al., 2002).

There is a growing amount of data supporting the origin of typical arc magmas via mantle melting fluxed by slab derived H_2O-rich component (e.g., Portnyagin et al., 2007b; Plank et al., 2013). According to these modern models, the compositions of primary magmas (including their H_2O and CO_2 contents) more likely result from an interplay of temperature and pressure of mantle melting with amount and composition of H_2O-bearing slab component. Fig. 5 presents an example of forward modeling of CO_2-Nb-H_2O relationships in arc magmas sourced from DMM, following the parameterization of fluxed melting of mantle peridotite taken from Portnyagin et al. (2007b). According to this model, the Klyuchevskoy

303 melts could have originated at 1.5 GPa and 1200 ^{o}C by ~11% melting of DMM fluxed by Nb-
304 free slab component with CO_2 ~3 wt.% and H_2O ~50 wt.%.

305 The example shown in Fig. 5 also illustrates that CO_2 content in primary arc magmas
306 should be quite variable and dependent on a number of parameters, such as initial mantle
307 source fertility, mantle temperature and pressure, and amount and composition of slab
308 component. The experimental approach adopted in this study can help to obtain more data
309 to establish global systematics for CO_2 in arc magmas and possibly to find some correlations
310 between the CO_2 content in magmas and geodynamic parameters of subduction zones.

311

312 **5.2 Effect of dehydration on homogenization of melt inclusions**

313 Experimental homogenization of MIs at 1 atm pressure has been conventionally
314 applied to determine composition of magma and its crystallization temperature (see reviews
315 by Roedder, 1984; Danyushevsky et al., 2002). This technique has been successfully used to
316 study primitive olivine-hosted MIs from different tectonic settings containing up to a few
317 wt.% H_2O (e.g., Sobolev and Danyushevsky, 1994; Sobolev and Chaussidon, 1996). However,
318 the results of our experimental study, as well as of the previous studies focusing on the
319 Klyuchevskoy MIs (Sobolev and Chaussidon, 1996; Portnyagin et al., 2007b; Churikova et al.,
320 2007; Mironov and Portnyagin, 2011), have demonstrated that simple increase of
321 experimental temperature up to 1400 ^{o}C is not sufficient to achieve complete
322 homogenization of the inclusions at 1 atm pressure.

323 Microthermometric experiments with subduction-related H_2O-rich MIs have
324 demonstrated that homogenization temperatures (T_{hom}) can increase by as much as 200 ^{o}C,
325 if these MIs are kept at a temperature >1100 ^{o}C for a few hours (e.g., Sobolev and
326 Danyushevsky, 1994; Danyushevsky et al., 2002; Massare et al., 2002). This was explained by

H_2O loss from MIs via diffusion of protons or water-bearing species (H_2O, OH^-) through the olivine lattice. Because the molar volume of H_2O dissolved in melt is large (Ochs and Lange, 1999), H_2O loss has a large effect on the density of melt (Fig. 4d) and, consequently, on T_{hom} (Sobolev and Danyushevsky, 1994). Massare et al. (2002) reported a correlation between the increase of T_{hom} from 1230 to 1405 ^oC and the decrease of *in-situ* measured H_2O content from 2.3 to 0.56 wt.% in MIs from the Stromboli volcano. According to these data, the loss of 1 wt.% H_2O from MIs is responsible for an increase of T_{hom} by ~100 ^oC due to the increase of density of the dehydrated melt and inward olivine crystallization.

Olivine phenocrysts used in our experiments were separated from lava samples, which were shown to have lost >3 wt.% H_2O due to slow cooling after eruption (Portnyagin et al., 2008; Mironov and Portnyagin, 2011). Applying the data from Massare et al. (2002) to the Klyuchevskoy MIs, we estimate that the loss of 3 wt.% H_2O would result in an increase of T_{hom} by >300 °C relative to the entrapment temperature of the inclusions (1150-1230 ^oC; Fig. 3, Table A.1). Therefore the expected T_{hom} of the dehydrated inclusions should be >1450 ^oC. None of the "dry" experiments in the present or previous studies on Klyuchevskoy MIs have been performed at such high temperature, and therefore no complete homogenization under dry conditions has been achieved.

The increase of external pressure to 300 MPa in dry experiments had a small effect on the reduction of fluid bubble volume (Fig. 4, Table 1, experiment #C8-5). This is in general agreement with the low compressibility of olivine and the prediction of about 0.08% reduction of olivine volume due to the increase of external pressure by 100 MPa (Handbook of physical constants, 1966). Thus, experimental heating at 1 atm or under confining pressure in the absence of a water-bearing medium is not an effective technique to overwhelm the large effect of H_2O loss and achieve complete homogenization of dehydrated

MIs. The experimental procedure adopted in this study was to produce re-hydration of MIs and to reach their homogenization at high H_2O pressure.

5.3 Homogenization of melt inclusions via experimental hydration

Experimental studies have shown that H diffusion in olivine is very fast (Kohlstedt and Mackwell, 1998; Demouchy and Mackwell, 2006; Portnyagin et al., 2008; Chen et al., 2011; Gaetani et al., 2012, 2014; Bucholz et al., 2013), and thus experimental de- and re-hydration of MIs trapped in olivine is possible on the time-scale of hours. Our present results confirm fast diffusion of proton in olivine at magmatic temperatures. During the relatively short time of our experiments (24 hours), initially "dry" inclusions were hydrated to contain 3.3-5.4 wt.% H_2O, which corresponds to 60-100% re-equilibration relative to the water content in the matrix melt (Table 1). Thus, the complete equilibration between MIs and water-bearing melt or fluid matrix may not have been achieved for the majority of melt inclusions during our 24 hours-long experiments. This observation is fully consistent with the diffusion coefficient of H_2O in olivine of ~$5*10^{-12}$ m^2/s at 1140-1164 ^oC (Portnyagin et al., 2008; Chen et al., 2011), which is slower than the proton-polaron diffusion (~$1*10^{-10}$ m^2/s at 1150 ^oC; Kohlstedt and Mackwell, 1998), and implies that, in our experiments, protons diffused together with octahedral metal (Mg and Fe) vacancies in olivine (Demouchy and Mackwell, 2006; Gaetani et al., 2012).

MIs in olivines in the experiments with a fluid matrix have significantly lower H_2O content compared to those with a matrix melt (Fig. 4, Table 1). Less efficient hydration of olivine and melt inclusions in the presence of fluid matrix is unexpected from proton-polaron diffusion but agrees well with a strong dependence of the rate of coupled proton-metal

vacancy diffusion on silica activity (Demouchy and Mackwell, 2006; Gaetani et al., 2014). The silica activity was presumably very low in the nominally Si-free fluid matrix.

The results of our experiments with hydrous melt as a source of water confirm the possibility to achieve complete homogenization by re-hydration of MIs at realistic magmatic temperatures that were estimated independently by thermometric approaches. As discussed above, loss of H_2O from MIs causes T_{hom} to increase dramatically. During experimental re-hydration, we simulated the inverse process and forced T_{hom} to decrease. Diffusion of H_2O into MIs decreased the density of the included melts (Fig. 4d) and also promoted melting of olivine from inclusion walls (Fig. 4c). Under near-isochoric and near-isothermal conditions, decrease in melt density and olivine melting resulted in an increase of the internal pressure (Fig. 4e) and CO_2 solubility in the melt (Fig. 4b), as well as efficient dissolution of the fluid bubble (Fig. 4a) until complete homogenization was achieved (Fig. 4a).

5.4 Interpretation of CO_2 and H_2O systematics in natural MIs

Two fundamentally different types of processes occurring either on the scale of magmatic systems or locally in MIs have been proposed to explain the combined systematics of H_2O and CO_2 in MI glasses. Variations of H_2O and CO_2 in MIs may reflect natural variability of initially trapped melts, resulting from magma degassing in open or closed systems, as well as from magma re-equilibration with fluid originating from deeper depths (gas flushing) (e.g. Metrich and Wallace, 2008). Significant variations of H_2O and CO_2 in MIs can also result from post-entrapment modification of inclusions such as a post-entrapment crystallization (PEC; Anderson and Brown, 1993; Steele-MacInnes et al., 2011) and dehydration (DH; Mironov and Portnyagin, 2011; Gaetani et al., 2012; Bucholz et al., 2013; this study). In addition, a

common process of Fe-loss from MIs (Danyushevsky et al., 2000) should be considered as a parameter affecting H_2O and CO_2 concentrations in the glass of olivine-hosted MIs, because it involves the exchange of MgO and FeO, which have slightly different molar volumes (Lange and Carmichael, 1990), and promotes olivine crystallization at isothermal conditions (Danyushevsky et al., 2000). The compositional trends, corresponding to the variety of processes, outline a triangular field in H_2O vs. CO_2 coordinates as illustrated in Fig. 6a (grey field). Analysis and interpretation of the trends in this field can be used to explain even very scattered H_2O and CO_2 contents in MIs from single rock samples.

The H_2O-CO_2 trend of post entrapment crystallization (PEC) is expected to have a curved, negatively-sloped shape for olivine-hosted inclusions but it was not modelled quantitatively thus far (Steele-MacInnes et al., 2011; Moore et al., 2015). Because the amount of H_2O in the fluid bubble formed by PEC is very small (Steele-MacInnes et al., 2011), the effect of PEC on H_2O concentration in the glass can be effectively corrected by modelling olivine crystallization. The corrected PEC trend (PEC* in Fig. 6a) displays constant H_2O over a wide range of CO_2 in the melt.

The effect of MI dehydration (DH) on CO_2 content of the melt is not well known (Mironov and Portnyagin, 2011; Gaetani et al., 2012; Bucholz et al., 2013). The results of our study suggest that the isothermal hydration (or dehydration) trend is nearly linear with x-y-intercepts close to zero in H_2O-CO_2 coordinates (High-T DH trend in Fig. 6). If dehydration occurs after MI cooling, the trend should be shifted to lower CO_2 concentrations as it involves PEC (Low-T DH trend in Fig.6). Why the experimentally produced (de)hydration trend should be linear and whether the trend is linear at lower temperatures is not fully understood yet. The problem should be investigated in more detail experimentally and theoretically. Nevertheless, the semi-quantitative effects are clear and can help to interpret

422 H_2O-CO_2 systematics of natural MIs. It is worth emphasizing that the dehydration and PEC
423 trends outline a triangular field in the CO_2-H_2O diagram, which encloses all possible trends
424 for magma degassing and gas flushing. The overlapping effects make it difficult to distinguish
425 the processes using the H_2O-CO_2 systematics alone (Fig. 6a).

426 Major and trace element compositions of MIs and their host minerals can help to
427 distinguish between the processes of magma degassing and gas flushing in contrast to post-
428 entrapment modification. The loss of H_2O from magma at subliquidus conditions (which are
429 required to trap inclusions in minerals) should ultimately result in crystallization. Therefore,
430 decreasing H_2O content in MIs due to magma degassing or flushing with CO_2-rich fluids
431 should generate a wide compositional range in the MIs and their host minerals, both
432 becoming more evolved with decreasing H_2O content. In contrast, MI dehydration and PEC
433 do not change the composition of the host mineral. Accounting for these effects,
434 interpretation of H_2O-CO_2 systematics can be significantly simplified, provided that co-
435 genetic inclusions with a narrow compositional range are selected. For MIs at the same stage
436 of magmatic crystallization, large variations of CO_2 and H_2O contents in the MI glasses should
437 be related to post-entrapment modification. Three examples of CO_2-H_2O systematics in co-
438 genetic MIs in olivine with a narrow Fo range are shown in Fig. 6b-d.

439 Glassy inclusions in olivine (Fo_{88-90}) from the Bulochka tephra (Auer et al. 2009 and
440 this study) contain 2.7-3.3 wt.% H_2O and 490-1170 ppm CO_2 (corrected for PEC) (Fig. 6b).
441 Both H_2O and CO_2 contents in these MIs are lower than those in the experimentally
442 homogenized MIs and in the Klyuchevskoy parental melts estimated independently (Mironov
443 and Portnyagin, 2011). The glass compositions fall within the triangle formed by PEC* and
444 high-T dehydration trends. Two-stage or simultaneously (dotted line in Fig. 6b) operating

445 processes of PEC and MI dehydration during magma cooling and degassing at shallow depth
446 or during tephra cooling upon eruption can explain the data (Lloyd et al., 2013).

447 MIs in high-Fo olivine from Colima volcano basanites (Vigouroux et al., 2008) exhibit a
448 nearly linear trend, which mimics closely the trend expected for isothermal dehydration
449 produced in our experimental study (Fig. 6c). The concentrations of CO_2 and perhaps H_2O in
450 the parental Colima melt are thought to be higher than the reported concentrations in the
451 MIs, because of the presence of relatively large fluid bubbles (2.9 vol.%) in the most volatile-
452 rich inclusions (Vigouroux et al., 2008). Therefore, the inclusions have likely experienced
453 some PEC after entrapment and then dehydrated to different extents at near isothermal
454 conditions (Fig 6c). A statistically significant (r^2=0.26 at the 95% confidence level, n=26)
455 positive correlation between the MI diameter and the amount of H_2O in the Colima
456 inclusions strongly supports this interpretation, because small inclusions dehydrate faster
457 than the larger ones (Qin et al., 1992; Lloyd et al., 2013). The amounts of H_2O in the
458 inclusions do not, however, correlate with the bubble sizes (0-8 vol.%) and therefore cannot
459 be explained by dehydration, necessitating further investigation.

460 MIs in olivine Fo_{90-91} from Etna volcano (Kamenetsky et al., 2007) define a crude
461 steep, positively sloped trend in H_2O-CO_2 diagram (Fig. 6d). The most H_2O- and CO_2-rich MIs
462 could have only experienced a minor amount of PEC and possibly up to 1 wt.% H_2O loss.
463 Three inclusions display low H_2O and CO_2 contents. They have the same major and trace
464 element composition as the H_2O-rich MIs and likely result from a larger extent of PEC and
465 dehydration processes. These MIs were likely extracted from a larger-size tephra clast or the
466 host crystals arrived in a different magma batch which has cooled slower compared to the
467 clasts/magma hosting olivines with H_2O-rich inclusions (Lloyd et al., 2013).

468

5.5 Experimental reconstruction of the initial composition of melt inclusions

The examples in Fig. 6 illustrate that MIs in high-Fo olivines usually experience significant post-entrapment modification of H_2O and CO_2 contents. Determination of the initially trapped melt composition is a problem, which cannot be solved solely by the analysis of modified inclusions, especially with regard to the initial H_2O content. Although our study was not specifically designed to estimate the initial H_2O content in the Klyuchevskoy melts, our results are nonetheless very promising in this direction.

As shown above (Sections 5.2 and 5.3), the conditions of complete homogenization (disappearance of fluid bubble) in the experiments are dependent on hydration, temperature and pressure. Increasing H_2O in MIs by 1 wt.% is approximately equivalent to an increase of the confining pressure by 650 MPa and to a temperature increase by 100 ^oC. Therefore, the conditions of complete homogenization of the Klyuchevskoy MIs obtained in this study are not unique. The complete homogenization of MIs could also be achieved at lower degree of hydration by increasing temperature and/or confining pressure.

In this study, complete homogenization of MIs in olivine Fo_{87-90} was achieved at 1150 ^oC and 500 MPa pressure, when the inclusions gained on average 4.5 wt.% H_2O. This amount is likely ~0.5 wt.% too high for the initial Klyuchevskoy melts (Mironov and Portnyagin, 2011), and the experimental temperature is about 50 ^oC lower than the crystallization temperature of the high-Fo Bulochka olivines (~1200 ^oC, Fig. 3a). Taking the effect of H_2O on homogenization temperature into account, the inclusions could be homogenized at ~4 wt.% H_2O and 1200 ^oC, which seems to be more realistic for Klyuchevskoy volcano (Mironov and Portnyagin, 2011).

Based on this promising result, we propose that the initial H_2O content in MIs can be estimated by experimental homogenization of inclusions at high H_2O pressure. Experimental

493 P-T-fO_2 conditions corresponding to the conditions of melt entrapment must be estimated
494 independently. Pressure can be estimated from the density of the co-genetic fluid inclusions,
495 temperature from olivine-spinel (Wan et al., 2008) or olivine-melt (e.g. Mallmann and
496 O'Neill, 2013) thermometers utilizing slow diffusing elements, and oxygen fugacity from
497 olivine-spinel (Ballhaus et al., 1990) or olivine-melt (e.g., Mallmann and O'Neill, 2013)
498 oxibarometers. Whereas the pressure and temperature during experiments directly
499 influence T_{hom}, the correct oxygen fugacity is required to achieve a realistic total Fe content
500 in the melt and to ensure complete dissolution of sulfides in MIs. When these requirements
501 are fulfilled, experiments with different amounts of H_2O in the matrix melt should be
502 performed in order to establish a correlation between the H_2O content in MIs and fluid
503 bubble size and estimate the H_2O content in the melt when the fluid bubble disappears (Fig.
504 4a). The duration of experiments should be set to ensure complete H_2O re-equilibration
505 between matrix and MIs. The time necessary for re-equilibration of MIs and olivine of a
506 given size can be calculated with the help of the model of Qin et al (1992) and published
507 diffusion coefficients for the cation vacancy driven diffusion of H_2O (e.g., Chen et al., 2011;
508 Portnyagin et al., 2008). The time needed for complete re-equilibration of a 100 μm MI in 1
509 mm olivine is about 48 hours at 1150 ^{o}C. Implementation of this technique requires a
510 sufficient number of olivine grains with inclusions of presumably close compositions and
511 conditions of entrapment to perform a series of experiments with variable H_2O content in
512 the matrix.

513 More tests of the proposed approach are currently in progress and will be published
514 elsewhere. If the tests are successful, the experimental protocol proposed here can be
515 equally well applied to any type of volcanic rock with well-preserved, water-bearing or
516 completely dehydrated inclusions (as in this study). This approach could significantly

increase the number of samples with magnesian olivine available for study of volatile contents and could allow the investigation of ancient volcanic rocks, expanding our knowledge of volatile recycling further back in Earth history.

6. Conclusions

In order to determine the initial volatile contents in MIs, CO_2 stored in the fluid bubble of melt inclusions must be taken into account. This goal can be achieved by a novel method, which is based on experimental hydration of MIs at high temperature and pressure. In this study, the hydration-driven homogenization of olivine-hosted MIs from Klyuchevskoy volcano was obtained at 1150 ^{o}C and 500 MPa when the H_2O contents in the inclusions reached 3.9-4.9 wt.%. The inclusions homogenized by this method contain 3800±140 ppm CO_2 and have a CO_2/Nb ratio of ~3000, representing the highest values ever reported for subduction-related melt inclusions. This agrees well with the independent estimations of the compositions of primary arc magma inferred from magma emplacement rates and data on volcanic gas emission in arcs. The obtained data and modeling of mantle melting suggest that ~83% CO_2 in the Klyuchevskoy magmas is derived from the subducting slab. The H_2O-CO_2-rich fluid/melt with a CO_2/H_2O ratio of ~0.06 triggered mantle melting and enriched the Klyuchevskoy parental magmas in a number of fluid-mobile elements including carbon.

Our new experimental results indicate that isothermal dehydration produces linear trends between H_2O and CO_2 in MI glasses, which can help to evaluate the behavior of volatile components in natural MIs. The interpretation of our results and of previously published data indicates that MIs in high-Fo olivines from subduction-related settings are subjected to significant post-entrapment crystallization and dehydration, which can strongly

modify H_2O and CO_2 contents in the residual glasses, as compared to the initially trapped melts.

We demonstrate that laboratory homogenization of olivine-hosted melt inclusions at high H_2O pressure can be efficiently used to reconstruct the initial composition of melt inclusions with respect to CO_2, probably H_2O and major elements also, given that the P-T-fO_2 conditions of inclusion entrapment are independently estimated and set during the experiments. The approach should be equally well applicable to MIs in olivine from rapidly quenched tephras that have been commonly used in MI studies in recent years, as well as from slowly cooled lavas, where MIs can lose nearly all of their original H_2O.

Acknowledgements

We are grateful to S. Simakin and E. Potapov for SIMS trace element analyses in Yaroslavl; M. Thöner for assistance with electron microprobe in Kiel; S. Fanara, A. Husen, A. Stechern and F. Vetere for experimental assistance; R. Almeev, H. Behrens, V. Naumov, A. Sobolev and Y. Taran for helpful discussions. T. Plank, an anonymous reviewer and editor T. Mather are sincerely thanked for providing insightful comments and corrections to the earlier version of this manuscript. Experiments were performed under support of the DFG grant HO1337/29. The Russian Science Foundation grant № 14-17-00582 and RFBR grant № 12-05-01131 provided support to N.M. and M.P. during manuscript preparation. The analytical costs were covered through the GEOMAR Helmholtz Center funding.

REFERENCES

Almeev, R.R., Holtz, F., Koepke, J., Parat, P., Botcharnikov, R.E., 2007. The effect of H_2O on olivine crystallization in MORB: Experimental calibration at 200 MPa. American Mineralogist 92, 670-674.

565 Anderson, A.T., Brown, G.G., 1993. CO_2 contents and formation pressures of some Kilauean
566 melt inclusions. American Mineralogist 78, 794-803.
567 Ariskin, A.A., Barmina, G.S., Ozerov, A.Y., Nielsen, R.L., 1995. Genesis of high-alumina basalts
568 from Klyuchevskoi volcano. Petrology 3, 496-521.
569 Auer, S.L., Bindeman, I., Wallace, P., Ponomareva, V.V., Portnyagin, M., 2009. The Origin of
570 Hydrous, high-$\delta^{18}O$ voluminous volcanism: Diverse Oxygen Isotope Values and High
571 Magmatic Water Contents within the Volcanic Record of Klyuchevskoy Volcano,
572 Kamchatka, Russia. Contributions to Mineralogy and Petrology 157, 209-230,
573 doi:210.1007/s00410-00008-00330-00410.
574 Ballhaus, C., Berry, R.F., Green, D.H., 1990. Oxygen Fugacity Controls in the Earths Upper
575 Mantle. Nature 348, 437-440.
576 Blank, J.G., Brooker, R.A., 1994. Experimental studies of carbon dioxide in silicate melts;
577 solubility, speciation, and stable carbon isotope behavior. Reviews in Mineralogy and
578 Geochemistry 30(1), 157-186.
579 Bucholz, C.E., Gaetani, G.A., Behn, M.D., Shimizu, N., 2013. Post-entrapment modification of
580 volatiles and oxygen fugacity in olivine-hosted melt inclusions. Earth and Planetary
581 Science Letters 374, 145-155.
582 Chen, Y., Provost, A., Schiano, P., Cluzel, N., 2011. The rate of water loss from olivine-hosted
583 melt inclusions. Contributions to Mineralogy and Petrology 162, 625-636.
584 Churikova, T., Wörner, G., Mironov, N., Kronz, A., 2007. Volatile (S, Cl and F) and fluid mobile
585 trace element compositions in melt inclusions: implications for variable fluid sources
586 across the Kamchatka arc. Contrib. Mineral. Petrol. 154, 217-239.

587 Danyushevsky, L.V., Della-Pasqua, F.N., Sokolov, S., 2000. Re-equilibration of melt inclusions
588 trapped by magnesian olivine phenocrysts from subduction-related magmas:
589 petrological implications. Contrib. Mineral. Petrol. 138, 68-83.
590 Danyushevsky, L., McNeill, A.W., Sobolev, A.V., 2002. Experimental and petrological studies
591 of melt inclusions in phenocrysts from mantle-derived magmas: an overview of
592 techniques, advantages and complications. Chemical Geology 183, 5-24.
593 Demouchy, S., Mackwell, S., 2006. Mechanisms of hydrogen incorporation and diffusion in
594 iron-bearing olivine. Physics and Chemistry of Minerals 33, 347-355.
595 Fischer, T.P., Marty, B., 2005. Volatile abundances in the sub-arc mantle: insights from
596 volcanic and hydrothermal gas discharges. Journal of Volcanology and Geothermal
597 Research 140, 205-216.
598 Gaetani, G.A., O'Leary, J.A., Shimizu, N., Bucholz, C.E., Newville, M., 2012. Rapid
599 reequilibration of H_2O and oxygen fugacity in olivine-hosted melt inclusions. Geology
600 40, 915-918.
601 Gaetani, G.A., O'Leary, J.A., Koga, K.T., Hauri, E.H., Rose-Koga, E.F., Monteleone, B.D., 2014.
602 Hydration of mantle olivine under variable water and oxygen fugacity conditions.
603 Contributions to Mineralogy and Petrology 167:965.
604 GEOROC, 2014. Geochemistry of rocks of the Oceans and Continents. MPI für Chemie,
605 Mainz, Germany. http://georoc.mpch-mainz.gwdg.de/georoc/
606 Handbook of physical constants, 1966. Clark, S.P., Jr, (Ed.). The geological society of America,
607 Yale University, New Haven, Connecticut.
608 Hartley, M.E., Maclennan, J., Edmonds, M., Thordarson, T., 2014. Reconstructing the deep
609 CO_2 degassing behaviour of large basaltic fissure eruptions. Earth and Planetary
610 Science Letters 393, 120-131.

611 Hilton, D.R., Fischer, T.P., Marty, B., 2002. Noble gases and volatile recycling in subduction
612 zones, in: Porcelli, D., Ballentine, C., Weiler, R. (Eds.), Noble gases in geochemistry
613 and cosmochemistry, Reviews in Mineralogy and Geochemistry. Miner. Soc. Am.,
614 Washington, D.C., pp. 319-370.
615 Kamenetsky, V.S., Davidson, P., Mernagh, T.P., Crawford, A.J., Gemmell, J.B., Portnyagin,
616 M.V., Shinjo, R., 2002. Fluid bubbles in melt inclusions and pillow-rim glasses: high-
617 temperature precursors to hydrothermal fluids? Chemical Geology 183, 349-364.
618 Kamenetsky, V.S., Pompilio, M., trich, N., Sobolev, A.V., Kuzmin, D.V., Thomas, R., 2007.
619 Arrival of extremely volatile-rich high-Mg magmas changes explosivity of Mount Etna,
620 pp. 255-258.
621 Kelemen, P.B., Hangøj, K., Greene, A.R., 2003. One view of the geochemistry of subduction-
622 related magmatic arcs, with and emphasis on primitive andesite and lower crust,
623 Treatise on Geochemistry. Elsevier, pp. 593-659.
624 Khubunaya, S.A., Bogoyavlenskiy, S.O., Novgorodtseva, T.Y., Okrugina, A.I., 1994. The
625 mineralogy of the Klyuchevskoi magnesian basalts depicting the fractionation in the
626 magma chamber. Volc. Seis. 15, 315-338.
627 Kohlstedt, D.L., Mackwell, S.J., 1998. Diffusion of hydrogen and intrinsic point defects in
628 olivine. Zeitschrift Fur Physikalische Chemie-International Journal of Research in
629 Physical Chemistry & Chemical Physics 207, 147-162, DOI:
630 110.1524/zpch.1998.1207.Part_1521_1522.1147.
631 Lange, R.L., Carmichael, I.S.E., 1990. Thermodynamic Properties of Silicate Liquids with
632 Emphasis on Density, Thermal-Expansion and Compressibility. Rev Mineral 24, 25-64.

633 Lloyd, A., Plank, T., Ruprecht, P., Hauri, E., Rose, W., 2013. Volatile loss from melt inclusions
634 in pyroclasts of differing sizes. Contributions to Mineralogy and Petrology 165, 129-
635 153.
636 Mallmann, G., O'Neill, H.S.C., 2013. Calibration of an Empirical Thermometer and
637 Oxybarometer based on the Partitioning of Sc, Y and V between Olivine and Silicate
638 Melt. J. Petrol. 54, 933-949.
639 Marty, B., Tolstikhin, I.N., 1998. CO_2 fluxes from mid-ocean ridges, arcs and plumes.
640 Chemical Geology 145, 233-248.
641 Massare, D., Metrich, N., Clocchiatti, R., 2002. High-temperature experiments on silicate
642 melt inclusions in olivine at 1 atm: inference on temperatures of homogenization and
643 H_2O concentrations. Chemical Geology 183, 87-98.
644 Metrich, N., Wallace, P.J., 2008. Volatile Abundances in Basaltic Magmas and Their Degassing
645 Paths Tracked by Melt Inclusions, in: Putirka, K.D., Tepley, F.J. (Eds.), Minerals,
646 Inclusions and Volcanic Processes. Reviews in Mineralogy & Geochemistry 69,
647 Mineralogical Soc Amer, Chantilly, pp. 363-402.
648 Mironov, N.L., Portnyagin, M.V., 2011. H_2O and CO_2 in parental magmas of Klyuchevskoy
649 volcano inferred from study of melt and fluid inclusions in olivine. Russian Geology
650 and Geophysics 52, 1353-1367.
651 Moore, L.R., Gazel, E., Tuohy, R., Lloyd, A.S., Esposito, R., Steele-MacInnis, M., Hauri, E., H.,
652 Wallace Paul, J., Plank, T., Bodnar, R., J., 2015. Bubbles matter: An assessment of the
653 contribution of vapor bubbles to melt inclusion volatile budgets, Am. Mineral., 806-
654 823.
655 Naumov, V.B., Portnyagin, M.V., Tolstykh, M.L., Yarmolyuk, V.V., 2006. Chemical
656 Composition and Crystallization Conditions of Trachybasalts from the Dzhida Field,

657 Southern Baikal Volcanic Area: Evidence from Melt and Fluid inclusions.
658 Geochemistry International 44, 286-295.
659 Newman, S., Lowenstern, J.B., 2002. VolatileCalc: a silicate melt H_2O-CO_2 solution model
660 written in visual basic for excel. Computers & Geosciences 28, 597-604.
661 Ochs, F.A., Lange, R.A., 1999. The Density of Hydrous Magmatic Liquids. Science 283, 1314-
662 1317, doi: 1310.1126/science.1283.5406.1314.
663 Plank, T., Kelley, K.A., Zimmer, M.M., Hauri, E.H., Wallace, P.J., 2013. Why do mafic arc
664 magmas contain ~4 wt.% water on average? Earth Planet. Sci.Lett. 364, 168-179.
665 Portnyagin, M., Almeev, R., Matveev, S., Holtz, F., 2008. Experimental evidence for rapid
666 water exchange between melt inclusions in olivine and host magma. Earth and
667 Planetary Science Letters 272, 541-552, doi:510.1016/j.epsl.2008.1005.1020.
668 Portnyagin, M., Bindeman, I., Hoernle, K., Hauff, F., 2007a. Geochemistry of primitive lavas
669 of the Central Kamchatka Depression: Magma Generation at the Edge of the Pacific
670 Plate, in: Eichelberger, J., Gordeev, E., Kasahara, M., Izbekov, P., Lees, J. (Eds.),
671 Volcanism and Subduction: The Kamchatka Region. American Geophysical Union,
672 Washington D.C., pp. 203-244.
673 Portnyagin, M.V., Hoernle, K., Plechov, P.Y., Mironov, N.L., Khubunaya, S.A., 2007b.
674 Constraints on mantle melting and composition and nature of slab components in
675 volcanic arcs from volatiles (H_2O, S, Cl, F) and trace elements in melt inclusions from
676 the Kamchatka Arc. Earth and Planetary Science Letters 255, 53-69.
677 Putirka, K.D. 2008. Thermometers and Barometers for Volcanic Systems, Minerals, Inclusions
678 and Volcanic Processes, in: Putirka, K.D., Tepley, F.J. (Eds.), Minerals, Inclusions and
679 Volcanic Processes. Reviews in Mineralogy & Geochemistry 69, Mineralogical Soc
680 Amer, Chantilly, pp. 61-120.

681 Qin, Z., Lu, F., Anderson Jr., A.T., 1992. Diffusive reequilibration of melt and fluid inclusions.
682 American Mineralogist 77, 565-576.
683 Roedder, E., 1984. Fluid inclusions. Miner.Soc.Amer., Michigan: Book Crafters Inc., 644 pp.
684 Rosenthal, A., Hauri, E.H., Hirschmann, M.M., 2015. Experimental determination of C, F, and
685 H partitioning between mantle minerals and carbonated basalt, CO_2/Ba and CO_2/Nb
686 systematics of partial melting, and the CO_2 contents of basaltic source regions. Earth
687 and Planetary Science Letters 412, 77-87.
688 Sadofsky, S., Portnyagin, M., Hoernle, K., van den Bogaard P., 2008. Subduction cycling of
689 volatiles and trace elements through the Central American volcanic arc: evidence
690 from melt inclusions. Contributions to Mineralogy and Petrology. 155: 433–456.
691 Schuessler, J.A., Botscharnikov, R.E., Behrens, H., Misiti, V., Freda, C., 2008. Oxidation state
692 of iron in hydrous phono-tephritic melts. American Mineralogist 93, 1493-1504.
693 Shaw, A.M., Behn, M.D., Humphris, S.E., Sohn, R.A., Gregg, P.M. 2010. Deep pooling of low
694 degree melts and volatile fluxes at the 85 degrees E segment of the Gakkel Ridge:
695 Evidence from olivine-hosted melt inclusions and glasses, Earth and Planetary Science
696 Letters 289, 311-322.
697 Shinohara, H., 2013. Volatile flux from subduction zone volcanoes: Insights from a detailed
698 evaluation of the fluxes from volcanoes in Japan. Journal of Volcanology and
699 Geothermal Research 268, 46-63, DOI: 10.1016/j.jvolgeores.2013.1010.1007.
700 Shishkina, T.A., Botcharnikov, R.E., Holtz, F., Almeev, R.R., Portnyagin, M.V., 2010. Solubility
701 of H_2O and CO_2-bearing fluids in tholeiitic basalts at pressures up to 500 MPa.
702 Chemical Geology, 115-125, doi:110.1016/j.chemgeo.2010.1007.1014.

Sobolev, A.V., Chaussidon, M., 1996. H_2O concentrations in primary melts from island-arcs and mid-ocean ridges: Implications for H_2O storage and recycling in the mantle. Earth and Planetary Science Letters 137, 45-55.

Sobolev, A.V., Danyushevsky, L.V., 1994. Petrology and Geochemistry of Boninites from the North Termination of the Tonga Trench: Constraints on the Generation Conditions of Primary High-Ca Boninite Magmas. Journal of Petrology 35, 1183-1211.

Steele-Macinnis, M., Esposito, R., Bodnar, R.J., 2011. Thermodynamic Model for the Effect of Post-entrapment Crystallization on the H_2O-CO_2 Systematics of Vapor-saturated, Silicate Melt Inclusions. Journal of Petrology 52-12, 2461-2482.

Vigouroux, N., Wallace, P.J., Kent, A.J.R., 2008. Volatiles in High-K Magmas from the Western Trans-Mexican Volcanic Belt: Evidence for Fluid Fluxing and Extreme Enrichment of the Mantle Wedge by Subduction Processes, pp. 1589-1618.

Wallace, P.J., 2005. Volatiles in subduction zone magmas: concentrations and fluxes based on melt inclusion and volcanic gas data. Journal of Volcanology and Geothermal Research 140, 217-240.

Wallace, P., Kamenetsky, V., Cervantes, P., 2015. Melt inclusion CO_2 contents, pressures of olivine crystallization and the problem of shrinkage bubbles. Am. Mineral., doi: 10.2138/am-2015-5029.

Wan, Z.H., Coogan, L.A., Canil, D., 2008. Experimental calibration of aluminum partitioning between olivine and spinel as a geothermometer. American Mineralogist 93, 1142-1147.

Workman, R.K., Hart, S.R., 2005. Major and trace element composition of the depleted MORB mantle (DMM). Earth Planet. Sci. Lett. 231, 53-72.

728 **Figure captions**

729 **Figure 1.** CO_2 concentrations in arc melt inclusions: (**a**) All melt inclusions from subduction-
730 related settings are from the GEOROC database (GEOROC, April 2014). Before this study, the
731 highest CO_2 content was measured in MIs from Etna (Kamenetsky et al., 2007) and Colima
732 (Vigouroux et al., 2008) volcanoes. (**b**) Olivine-hosted melt inclusions from volcanic rocks
733 from Klyuchevskoy Volcano rocks: natural glassy inclusions (Auer et al., 2009; Mironov and
734 Portnyagin, 2011; this study); reheated at 1 atm and 300 MPa without H_2O (Mironov and
735 Portnyagin, 2011; this study); and rehydrated at high H_2O pressure (300-500 MPa, this
736 study). The lowest expected CO_2 concentration in primary arc melts is shown (~3000 ppm
737 after Wallace, 2005). The most recent estimate of CO_2 in primary arc magmas (~3700 ppm) is
738 based on the ^3He flux and magmatic emplacement rate estimates at convergent margins
739 (Shinohara, 2013).
740
741 **Figure 2**. Typical Klyuchevskoy melt inclusions before and after the experiments.
742 (**a**) Fragment of typical olivine phenocryst from Bulochka tephra. (**b**) Glassy inclusion K6-mi2
743 (Table 1) from Bulochka tephra. (**c**) Dense fluid inclusion in olivine from Ochki lava flow from
744 Klyuchevskoy volcano. This inclusion has a CO_2 density of 0.81 g/cm^3 as estimated from the
745 homogenization temperature to liquid at 16.8 ^oC. The density corresponds to CO_2 pressure
746 of 530 MPa at 1200 ^oC and concentration of CO_2 in equilibrium melt of ~3500 ppm (Mironov
747 and Portnyagin, 2011). (**d**) Partially crystallized melt inclusion in high-Fo olivine from
748 Bulochka lava flow typical of those used for this experimental study. (**e**) Inclusion #C9-1 after
749 heating at 1400 ^oC and 1 atm in graphite capsule for 1 hour. (**f**) Inclusion #C8-5-3 after
750 experimental run at 1200^o C, 300 MPa and NNO buffer without H_2O for 28 hours. (**g**)
751 Inclusion #C4-4-2 after experimental run with fluid matrix (H_2O+20% NaCl) at 1150^o C, 300
752 MPa pressure and QFM+3.3 for 24 hours. (**h**) Inclusion #C4-2-1b after experimental run at
753 1150^o C, 300 MPa H_2O pressure and QFM+3.3 for 24 hours. (**i**) Homogeneous (no fluid phase)
754 inclusions #C10-2-4 after experimental run at 1150 ^oC, 500 MPa H_2O pressure and NNO for
755 24 hours. Small Cr-spinel crystals are interpreted to be prisoner phases. In panels (**b**, **e-i**)
756 concentrations of CO_2 and H_2O in glass are indicated in ppm and wt.%, respectively
757 ("620/0.14" refers to CO_2 = 620 ppm, H_2O = 0.14 wt.%). The volume of fluid bubbles ("Fluid")
758 is indicated in volume % relative to total volume of inclusions. Sulfide globules observed in
759 MIs after dry (no H_2O in matrix) experiments at QFM+0.6 and CCO (panels **e** and **f**) are

760 daughter phases resulting from sulfide saturation at these conditions. Note the decreasing
761 fluid bubble volume and the concomitantly increasing H_2O and CO_2 concentrations in glass
762 with increasing experimental H_2O pressure.
763
764 **Figure 3**. Fosterite content of olivine versus (a) temperature and (b) oxygen fugacity for
765 primitive Klyuchevskoy magmas (Bulochka, Ochki and Tuyla vents). **(a)** Temperature
766 estimated from Al partitioning between olivine and spinel (Wan et al., 2008). The
767 temperatures and their uncertainty (1 SD) are calculated from 4 olivine analyses around
768 spinel inclusions. **(b)** Oxygen fugacity (expressed as ΔQFM) estimated from olivine-spinel
769 equilibria (Ballhaus et al., 1990). Uncertainty of ΔQFM is assumed to be ~0.5 log units.
770 Dashed lines illustrate conditions of high-pressure experiments of this study. The
771 compositions of olivine and spinel and calculated values of T and fO_2 are given in Table A1.
772
773 **Figure 4.** Compositional and physical characteristics of MIs after experimental runs.
774 Measured (**a**) relative fluid bubble volume, (**b**) CO_2, (**c**) MgO and calculated (**d**) melt density,
775 (**e**) fluid saturation pressure and (**f**) mole fraction of CO_2 in fluid phase are plotted versus
776 H_2O content, which reflects the extent of MI hydration during the experiments. MIs treated
777 under anhydrous conditions (experiments #C8-5 and C9) represent the compositions of
778 dehydrated MIs before experiments (with respect to H_2O and CO_2 contents in glass). Linear
779 regression lines are calculated for the data sets. In plot (**b**) thin solid lines (NL2002) denote
780 isobars of H_2O-CO_2 solubility in melt at 100 to 500 MPa calculated using the VolatileCalc
781 program (Newman and Lowenstern, 2002). Bold gray line (500 MPa, SH2010) denotes the
782 500 MPa isobar for a basalt from Mutnovsky volcano (Kamchatka) after Shishkina et al.
783 (2010). Bold arrows labeled as “Low T, P” and “High T, P” illustrate the likely shift of the
784 homogenized MI composition as a result of changing P-T conditions of experiment (see text
785 for explanation). Dashed arrow illustrates the possible effect of isochoric post-entrapment
786 crystallization (PEC) on the composition of melt in MIs at decreasing ambient temperature
787 (Steele-MacInnes et al., 2011). In plot (**c**) isotherms for H_2O-saturated conditions were
788 calculated by using a simplified model of olivine-melt equilibria (Putirka, 2008; Eq. 14 solved
789 for melt Mg#=0.65, Na_2O+K_2O=3.5 wt.% and FeO=8.5 wt.%) relating olivine liquidus
790 temperature, MgO and H_2O contents in melt. We modified the model by taking the non-
791 linear effect of the amount of H_2O in the melt on the olivine liquidus T into account (Almeev

et al., 2007). An approximate amount of olivine dissolved in MIs during experiments was calculated assuming initial MgO=4 wt.% in the melt and is shown on the right side of the diagram. In plot (**d**), density of melt was calculated after Lange and Carmichael (1990) and Ochs and Lange (1999) at the experimental P-T conditions. In plots (**e**) and (**f**), fluid saturation pressure and mole fraction of CO_2 in fluid phase are calculated using VolcatileCalc from MI glass compositions. The estimates should be considered as semi-quantitative, providing information about the trend direction rather than absolute values, because VolatileCalc does not fully account for compositional effects on H_2O-CO_2 solubility (e.g. Shishkina et al., 2010) and is not recommended for P>500 MPa (Newman and Lowenstern, 2002). In plots (**b**) and (**f**) model trends for open system degassing (OD), for closed system degassing in a case with 1 wt.% vapor (CD), and for magma flushed with fluid containing 30 mol.% H_2O (FF) were calculated with Volatile Calc using a starting composition of 4.5 wt.% H_2O, 3800 ppm CO_2, 49 wt.% SiO_2 and T of 1150 ^oC. Error bars: H_2O - 9 rel.%, CO_2 - 17 rel.%, MgO - 0.5 wt.%, melt density - 0.05 g/cm^3 (assumed), pressure - 20% relative (assumed to account for difference between VolatileCalc and Shishkina et al. (2010) models); fluid bubble volume – propagated from ±1 μm uncertainty of bubble diameter measurements.

Figure 5. Nb-CO_2-H_2O systematics of olivine-hosted MIs from subduction-zone (SZ) volcanoes (open circles; n=338; GEOROC, 2014 and Appendix B) and homogenized MIs from Klyuchevskoy volcano (red circles). Depleted MORB mantle (DMM) composition is after Workman and Hart (2005) and Rosenthal et al. (2015). Lines represent compositions of partial melts produced by DMM melting fluxed by H_2O-bearing slab component (SC) as modeled following parameterization by Portnyagin et al. (2007b) and assuming bulk partition coefficients from Workman and Hart (2005) and Rosenthal et al. (2015). Light blue field denotes the compositional trend without slab input. Colored lines illustrate forward modeling of DMM melting at 1.5 GPa and temperatures of 1275 ^oC (dry peridotite solidus, solid green lines) and 1200 ^oC (75 ^oC below dry peridotite solidus, dashed blue lines) with different contribution from slab component having 50 wt.% H_2O and variable amount of CO_2 (0, 1, 3, 7, 20 wt.% CO_2 at 1275 ^oC , 0, 3 and 7 wt.% CO_2 at 1200 ^oC) as noted by corresponding labels. The best match of the modeled melts and the inferred compositions of primary Klyuchevskoy melts (1.3 ppm Nb, 3800 ppm CO_2, 4-5 wt.% H_2O; Mironov and

823 Portnyagin, 2011; this study) is achieved at ~11% melting at temperature 75 ^{o}C below dry
824 peridotite solidus.
825
826 **Figure 6.** Interpretation of CO_2 and H_2O systematics in natural glassy melt inclusions.
827 **(a)** Possible trajectories of melt evolution with initial 4.5 wt.% H_2O and 3800 ppm CO_2, which
828 can be recorded in MIs: OD – degassing in open system, CD - degassing in closed system
829 assuming 1 wt.% of vapor in magma; FF – magma flushed with fluid containing 30 mol.%
830 H_2O; PEC – approximate trend of post entrapment crystallization in MI; PEC* - PEC with H_2O
831 content corrected for the amount of crystallized host-mineral; High-T DH and Low-T DH –
832 high and low temperature dehydration of MIs, respectively. OD, CD and FF were calculated
833 using VolatileCalc (Newman and Lowenstern, 2002); PEC – qualitatively defined based on
834 data of Steele-MacInnes et al. (2011). PEC* is H_2O corrected PEC trend. Dehydration trends
835 are based on this study. **(b)** MIs from Bulochka tephra (*blue diamonds*) after Auer et al.
836 (2009) (sample KLV5/8) and this study. *Open circles* denote compositions of experimentally
837 treated MIs from this study. The H_2O content in the initially trapped Bulochka melts (*large*
838 *open circle with question mark*) is not known precisely and assumed to be 4 wt.% H_2O. The
839 CO_2 content is 3800 ppm (this study); **(c)** MIs from Colima basanites (Vigouroux et al., 2008);
840 **(d)** MIs from Etna (Kamenetsky et al., 2007). All MIs in plots (**b-d)** are natural glassy
841 inclusions trapped in high-Fo olivine with a narrow (1-2 mol.% Fo) range. The H_2O content in
842 MIs was corrected for PEC. Gray triangles outline the field of possible evolution of H_2O and
843 CO_2 in MI due to PEC and dehydration. Initially trapped compositions of MIs from Etna and
844 Colima are not known. Their minimal H_2O and CO_2 are shown by *open circles with question*
845 *mark* in the right upper corner of the triangle enclosing the MIs populations. Dotted curves
846 illustrate possible trends of simultaneously occurring PEC and dehydration. According to our
847 interpretation, the natural glassy MIs record variable extent of PEC and dehydration and do
848 not correspond in composition to the initially trapped melt. See text for more discussion.
849

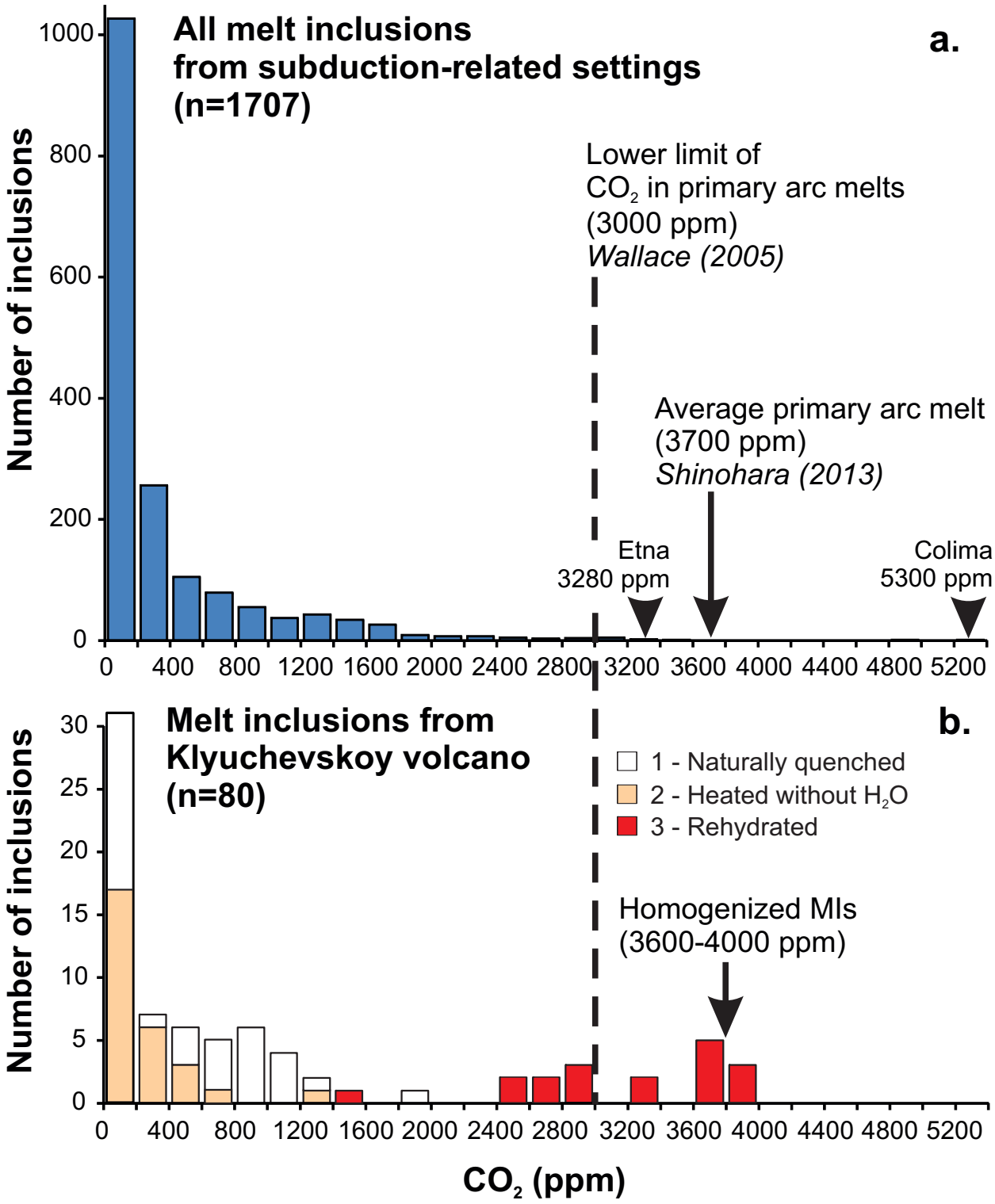

Fig.1
(Mironov et al.)

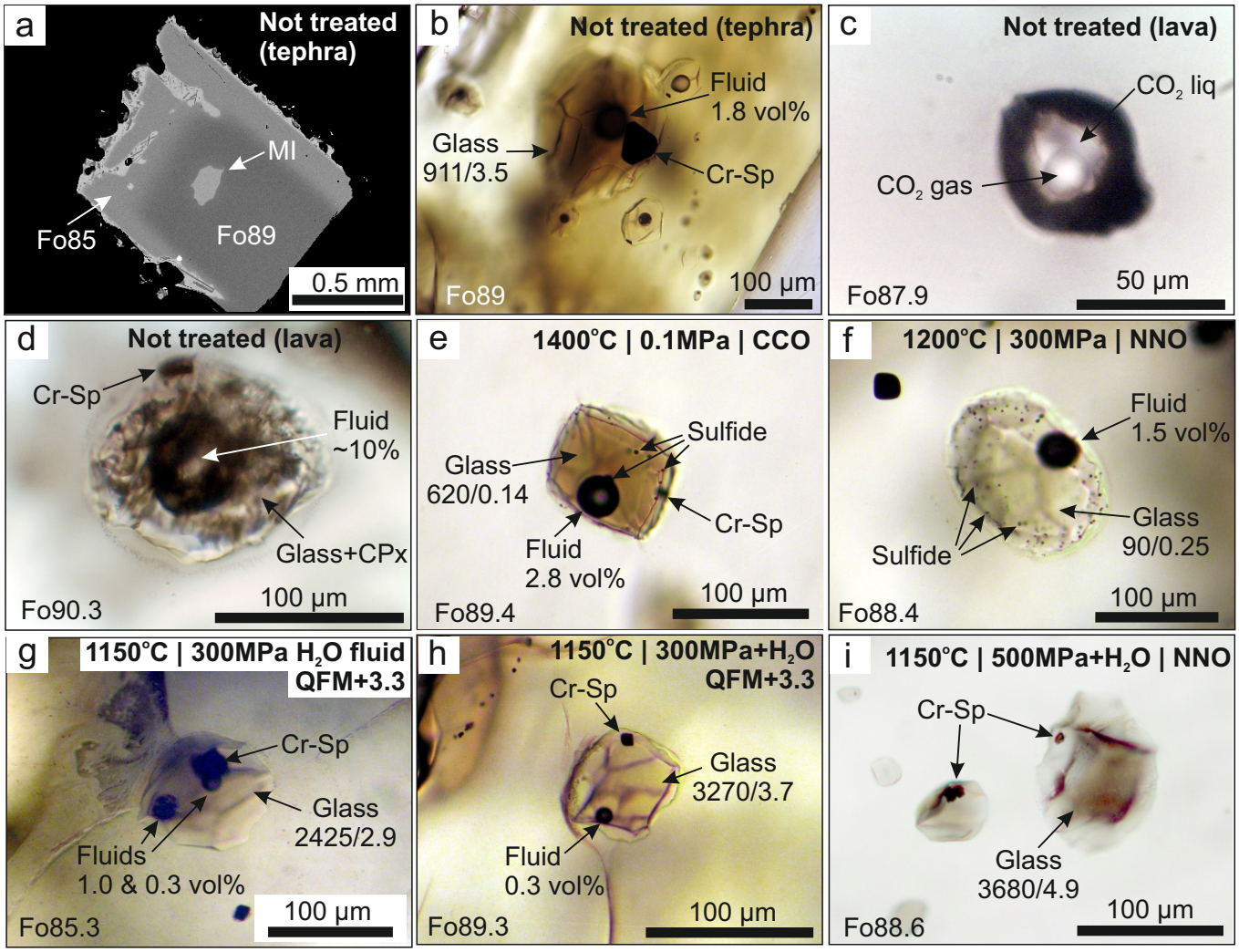

Fig.2
(Mironov et al.)

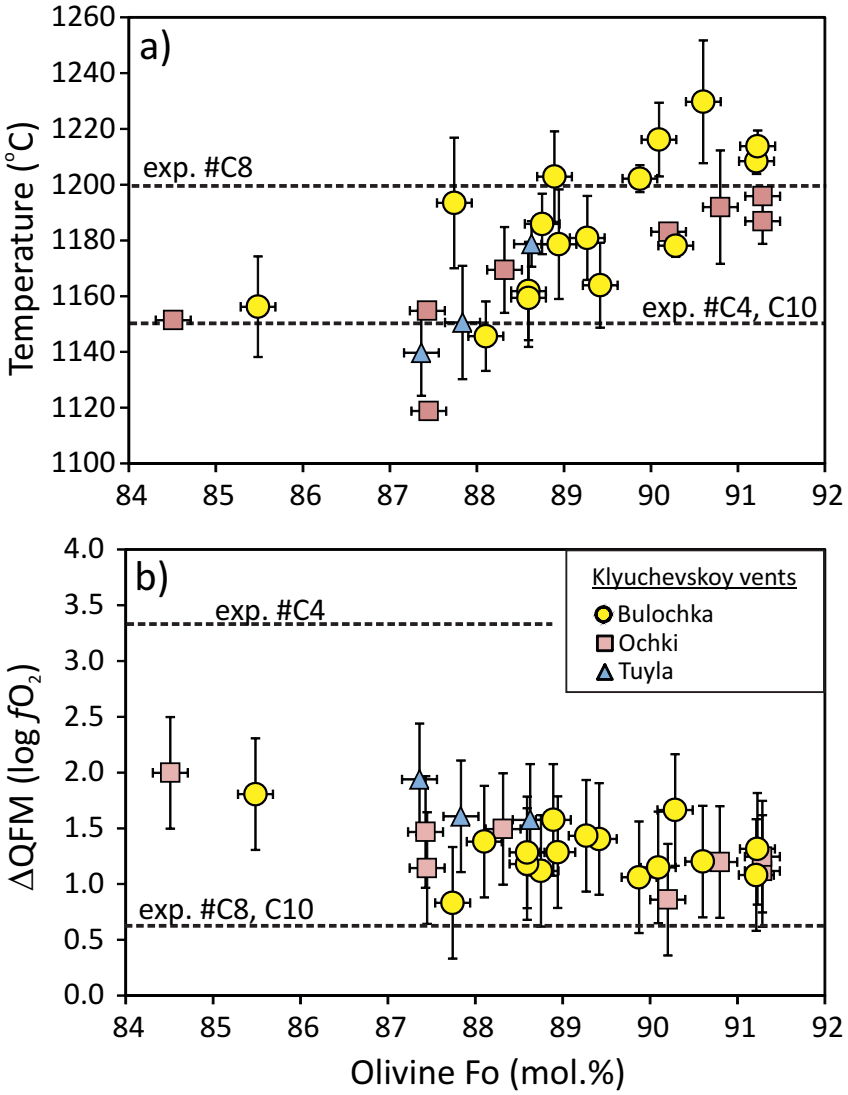

Fig. 3 (Mironov et al.)

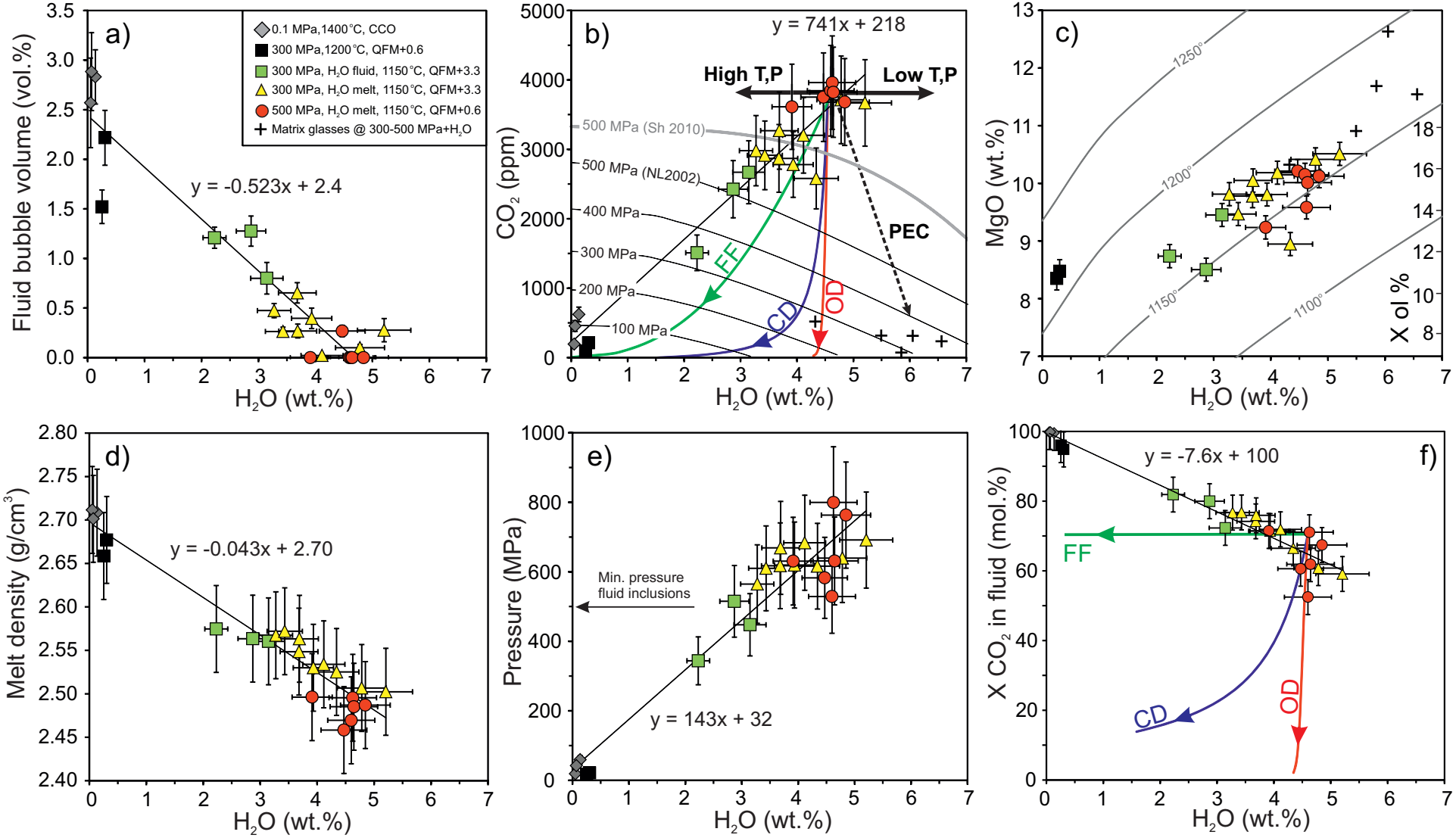

Fig. 4 (EPSL_13266) edited

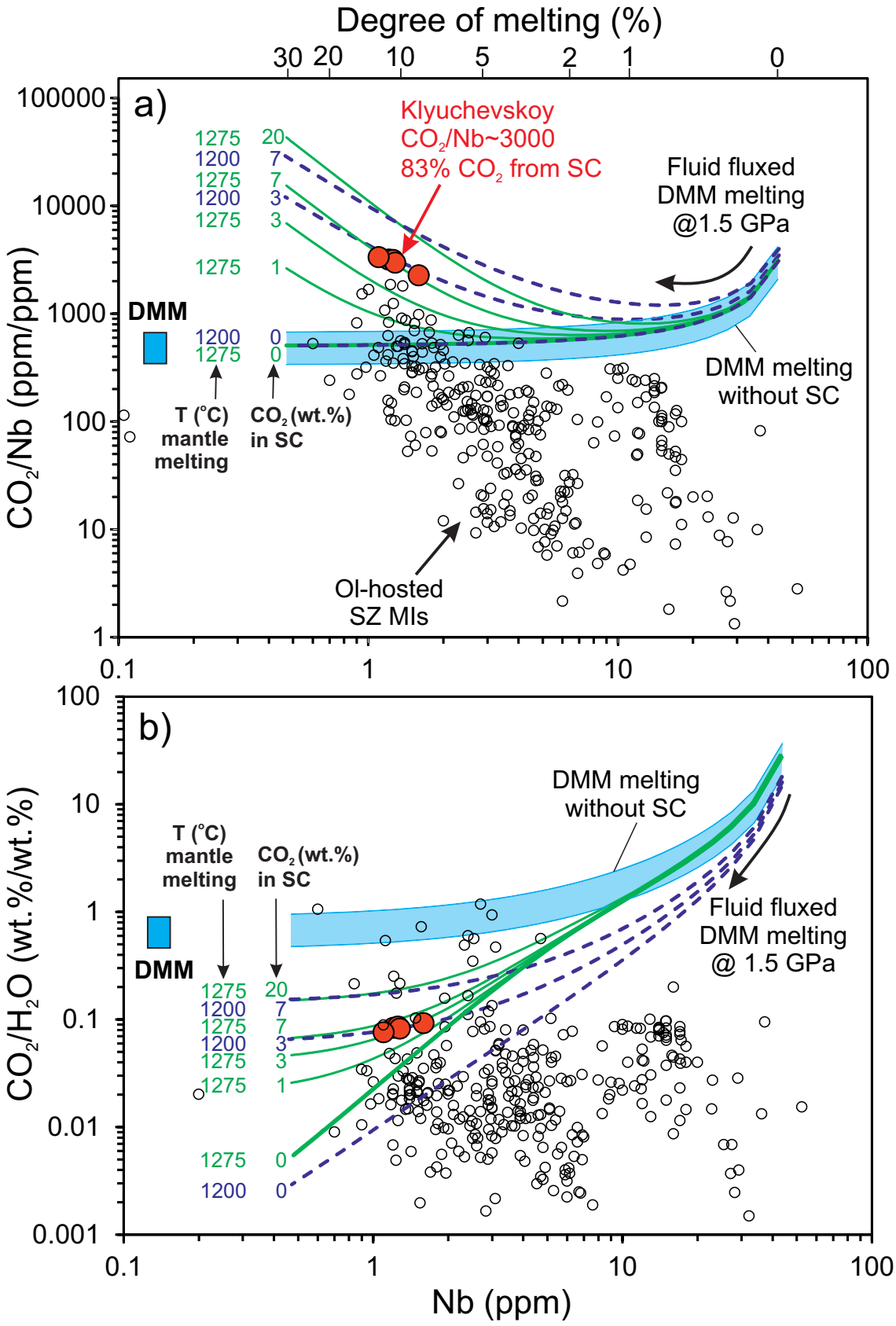

Fig. 5 (EPSL_13266) edited

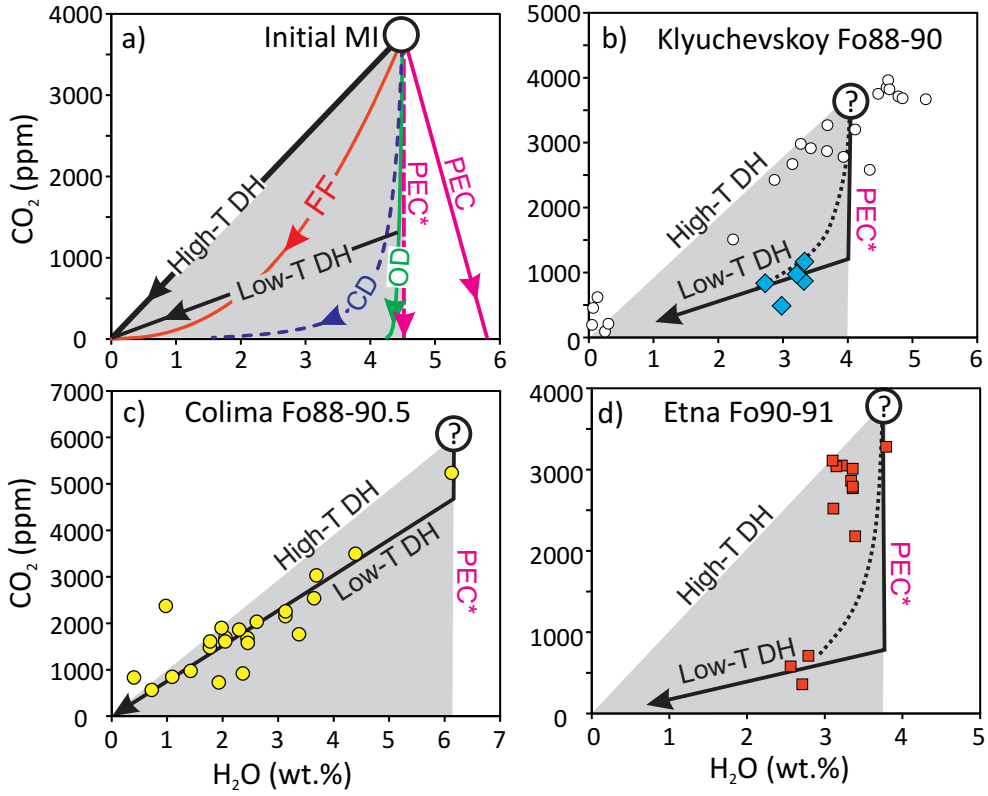

Fig. 6 (EPSL_13266) edited

Table 1. Experimental conditions, compositions of melt inclusions, matrix glasses and host-rocks

Exp #	Conditions	Sample #	Type	Phases in MI	D (μm)	FB (vol.%)	Fo (mol.%)	SiO_2	TiO_2	Al_2O_3	FeO	MnO	MgO	CaO	Na_2O	K_2O	P_2O_5	S	Cl	Total	CO_2	H_2O	Ba	Th	La	Nb
Starting matrix glass		KL-R	G					50.71	0.86	13.63	9.18	0.07	11.98	10.80	2.16	0.47	0.10			100.00						
Bulochka lava			WR					51.15	0.75	13.60	8.65	0.17	11.85	9.75	2.30	0.55	0.13			98.90			225	N/A	4.6	N/A
Bulochka tephra		K7-T1-51	WR					50.59	0.76	13.09	9.17	0.17	13.08	9.25	2.36	0.53	0.13			99.13			209	0.35	3.9	1.1
C4-1	300 Mpa, 1150 °C, 24h, QFM+3.3, matrix glass + 9.3% H_2O	C4-1-1	MI	g,f,sp	100	0.02	89.1	49.59	0.60	12.58	9.37	0.14	9.68	10.45	1.93	0.35	0.09	0.18	0.064	95.02	3202	4.12	159	0.15	2.7	0.8
		C4-1-2	MI	g,f	107	0.65	88.7	48.99	0.73	12.86	9.87	0.17	9.29	9.87	2.42	0.46	0.09	0.20	0.062	95.01	2869	3.68	195	0.30	3.9	1.2
		C4-1-3	MI	g,f	100	0.10	88.4	47.93	0.68	12.54	10.59	0.20	9.81	9.71	2.03	0.37	0.09	0.20	0.062	94.22	3713	4.78	152	0.25	3.2	1.1
		C4-1-G	G				91.8	48.58	0.75	12.16	8.47	0.08	10.88	9.61	2.01	0.44	0.10	0.00	0.006	93.07	71	5.85	2	0.01	0.1	0.9
C4-2	300 Mpa, 1150 °C, 24h, QFM+3.3, matrix glass + 5 % H_2O	C4-2-1a	MI	g,f,sp,cp	125	0.47	89.4	48.68	0.70	12.86	8.88	0.13	9.37	12.15	1.90	0.39	0.10	0.21	0.080	95.45	2980	3.27	189	0.18	3.4	1.0
		C4-2-1b	MI	g,f,sp	90	0.27	89.3	49.37	0.68	12.45	9.37	0.17	9.62	11.55	1.76	0.37	0.08	0.20	0.067	95.68	3269	3.69	173	0.19	3.2	0.9
		C4-2-2	MI	g,f,sp	79	0.40	89.6	49.56	0.74	12.99	9.27	0.15	9.37	10.36	2.22	0.53	0.12	0.17	0.054	95.53	2781	3.93	226	0.36	3.9	1.2
		C4-2-3b	MI	g,f,sp	41	N/A	87.6	49.10	0.80	12.33	12.01	0.16	8.49	8.60	2.51	0.58	0.14	0.13	0.048	94.90	2581	4.34	242	0.32	8.0	1.4
		C4-2-G	G				90.4	50.38	0.78	12.76	8.70	0.07	9.84	10.04	2.12	0.46	0.12	0.00	0.009	95.28	519	4.33	2.4	0.01	0.1	1.0
C4-3	300 Mpa, 1150 °C, 24h, QFM+3.3, matrix glass + 11.3% H_2O	C4-3-1	MI	g,f,sp	138	0.26	87.6	49.03	0.75	13.01	10.15	0.14	9.07	10.84	2.07	0.42	0.09	0.19	0.060	95.83	2914	3.43	194	0.23	3.9	1.2
		C4-3-2	MI	g,f	57	0.28	89.1	48.17	0.63	11.44	11.17	0.16	9.91	10.30	1.80	0.38	0.07	0.19	0.072	94.28	3669	5.21	166	0.18	3.2	0.9
		C4-3-G	G				92.9	49.54	0.73	12.51	8.71	0.12	10.28	9.42	2.05	0.77	0.11	0.00	0.001	94.25	316	5.49	2.0	0.01	0.2	0.9
C4-4	300 Mpa, 1150 °C, 24h, QFM+3.3, matrix H_2O + 20% NaCl	C4-4-2	MI	g,f,sp	112	1.28	85.3	50.48	0.74	14.34	10.05	0.17	8.18	8.75	2.65	0.46	0.11	0.20	0.067	96.17	2425	2.87	170	0.26	4.0	1.3
		C4-4-3	MI	g,f	153	1.21	90.0	49.37	0.86	14.80	7.83	0.12	8.50	12.26	2.60	0.53	0.10	0.23	0.078	97.29	1510	2.23	241	0.34	4.7	1.5
		C4-4-5	MI	g,f	80	0.80	89.3	47.98	0.68	14.25	9.06	0.12	9.09	12.09	2.12	0.40	0.08	0.19	0.076	96.14	2670	3.15	184	0.27	3.7	1.0
C8-5	300 Mpa, 1200 °C, 28h, QFM+0.6, no matrix	C8-5-3	MI	g,f,s	113	1.52	88.4	48.68	0.97	17.64	7.29	0.15	8.37	13.34	2.86	0.61	0.14	0.08	0.074	100.21	90	0.25	279	0.37	5.2	1.6
		C8-5-4a	MI	g,f,s	89	2.22	88.7	46.22	1.03	18.58	7.23	0.11	8.50	14.61	3.13	0.57	0.13	0.12	0.110	100.32	211	0.30	228	0.33	4.8	1.5
C9	1 atm, 1400°C, 1 h, CCO, no matrix	C9-1	MI	g,f,s	105	2.83	89.4	46.16	0.77	13.31	8.85	0.17	15.97	12.61	2.00	0.40	0.07	0.21	0.073	100.58	621	0.14	206	0.28	3.8	1.1
		C9-2	MI	g,f,s,sp	61	2.57	88.8	46.33	0.80	13.22	9.45	0.15	15.82	12.11	2.26	0.45	0.09	0.15	0.067	100.89	193	0.05	238	0.37	4.7	1.4
		C9-3	MI	g,f,s	75	2.88	89.7	46.04	0.88	13.79	8.86	0.14	15.59	11.23	2.26	0.45	0.11	0.16	0.066	99.58	456	0.07	216	0.27	4.8	1.5
C10-1	500 Mpa, 1150 °C, 24h, QFM+0.6, matrix glass + 11.1% H_2O	C10-1-1	MI	g,s,sp	108	0.27	90.9	47.45	0.84	14.75	5.77	0.10	9.50	10.71	2.71	0.52	0.10	0.17	0.111	93.00	3752	4.47	186	0.21	4.0	1.5
		C10-1-2	MI	g,sp	100	0	87.7	46.15	1.06	14.61	8.10	0.15	9.46	9.54	2.78	0.66	0.13	0.18	0.059	93.22	3845	4.60	259	0.44	4.5	1.2
		C10-1-3	MI	g,s	116	0	86.6	48.97	0.84	14.25	7.70	0.13	9.00	9.14	2.78	0.53	0.12	0.13	0.062	93.90	3961	4.63	170	0.16	3.9	1.3
		C10-1-3-G	G				91.1	48.01	0.74	11.96	6.15	0.05	11.43	9.67	1.98	0.51	0.11	0.00	0.008	90.47	312	6.05	N/A	N/A	N/A	N/A
C10-2	500 Mpa, 1150 °C, 24h, QFM+0.6, matrix glass + 5.6 % H_2O	C10-2-1	MI	g,s,sp	106	0	87.3	47.82	0.75	13.12	7.76	0.16	9.39	11.58	2.27	0.43	0.10	0.14	0.067	93.83	3822	4.64	188	0.20	3.6	1.3
		C10-2-2a	MI	g,s,sp,px	118	0	89.7	48.44	0.90	14.93	6.18	0.11	8.72	10.96	3.12	0.56	0.13	0.11	0.074	94.46	3612	3.91	209	0.21	4.2	1.6
		C10-2-4	MI	g,sp	92	0	88.6	48.90	0.80	13.14	7.60	0.14	9.49	10.50	2.24	0.42	0.12	0.15	0.058	93.78	3681	4.85	140	0.20	3.1	1.1
		C10-2-4-G	G				91.2	49.41	0.78	12.33	5.79	0.09	10.60	10.11	2.14	0.46	0.09	0.00	0.003	91.81	235	6.56	N/A	N/A	N/A	N/A
K7-T1-51	Natural	K6-mi1	MI	g,f,sp	88	2.33	89.0	49.40	0.89	15.35	6.58	0.13	7.07	12.97	2.67	0.53	0.10	0.19	0.071	96.28	879	2.87	223	0.31	5.1	1.5
		K6-mi2	MI	g,f,sp	288	1.78	89.0	49.36	0.87	14.75	7.04	0.13	7.39	12.67	2.55	0.51	0.10	0.18	0.069	95.92	911	3.49	206	0.22	4.1	1.4
		K7-mi	MI	g,f,sp	80	2.70	85.1	48.78	1.02	15.55	8.06	0.16	6.68	10.83	2.84	0.64	0.11	0.18	0.061	95.22	934	3.09	239	0.27	4.3	1.6
		K16-mi	MI	g,f,sp	178	1.14	87.9	48.94	0.91	15.63	6.98	0.15	6.78	12.12	2.63	0.54	0.12	0.24	0.083	95.48	1198	3.42	203	0.27	3.8	1.5

Notes:
Type: MI-melt inclusion, G - matrix glass, WR - whole rock;
Phases: g - glass, f - fluid, s - sulfide, sp - Cr-spinel, px - clinopyroxene;
D - average two-dimentional diameter of melt inclusion;
FB - relative volume of fluid bubble (vol.%);
Fo - Fo of host olivine for inclusions, Fo from matrix or crystal faces for matrix glass;
Major elements, S, and Cl - EMP data (wt.%);
CO_2 and H_2O - SIMS data (CRPG, Nancy) (ppm and wt.%);
Ba, Th, La, Nb - SIMS data (YBIFT,Yaroslavl) (ppm);
Matrix glass KL-R was synthesized from pure oxides (provided by R.Almeev);
Bulochka tephra sample K7-T1-51 was analysed by XRF and ICP-MS in GEOMAR, Kiel;
Bulk rock Bulochka lava composition is after Ariskin et al. (1995) (averaged from two analyses, KL-3 and KL-5);
Nominal redox conditions in C4 experimental series were at QFM+3.3, but in C4-2 could be slightly more reduced (<0.5 log units fO_2),
because water content in the matrix melt was lower than the solubility of water at given pressure resulting in lower water activity.